

In situ nanoscale mapping of the chemical composition of surfaces and 3D nanostructures by photoelectron spectromicroscopy

Fulvio Ratto^{1,2}, Stefan Heun^{3,5}, Oussama Moutanabbir⁴ and Federico Rosei^{1,5}

¹ Institut National de la Recherche Scientifique—Energie, Matériaux et Télécommunications (INRS-EMT), Université du Québec, 1650 Boulevard Lionel Boulet, J3X 1S2 Varennes, QC, Canada

² Istituto di Fisica Applicata, Consiglio Nazionale delle Ricerche (CNR-IFAC), Via Madonna del Piano 10, I-50019 Sesto Fiorentino, Italy

³ NEST CNR-INFN and Scuola Normale Superiore, Via della Faggiola 19, 56126 Pisa, Italy

⁴ Max Planck Institute of Microstructure Physics, Halle (Saale), D 06120, Germany

E-mail: stefan.heun@sns.it and rosei@emt.inrs.ca

Received 14 February 2008, in final form 22 April 2008

Published 20 May 2008

Online at stacks.iop.org/Nano/19/265703

Abstract

We propose a novel approach to extract quantitative chemical maps of surfaces with nanoscale resolution, from the analysis of data from x-ray photoemission electron microscopy, which is a minimally invasive technique. Our formulation allows us to extract chemical maps from the raw data even in cases when not all experimental parameters are well known or controlled. We illustrate our concept by the analysis of a ternary alloy with a nanoscale pattern, to achieve chemical maps of unprecedented quality.

(Some figures in this article are in colour only in the electronic version)

1. Introduction

The ability to map surface chemistry with nanoscale resolution is becoming increasingly crucial for an improved understanding of the properties and behaviour of nanostructures. In many cases the amazing functionalities of surface nanopatterns directly or indirectly follow from nanoscale inhomogeneities of chemical nature [1]. This is the case for example for heteroepitaxial quantum dots, where confinement of charge carriers occurs due to chemical segregation and strain [2–4]. Further examples include nanomolecular devices [1, 5], memories [6], catalysts [7], sensors [8], actuators, etc. However, in spite of this context, there are still only a few non-destructive methods available to extract quantitative and reliable information on chemical composition at the nanoscale [2].

Among the most promising approaches is photoelectron spectromicroscopy, such as synchrotron x-ray photoemission electron microscopy (XPEEM), which is a minimally invasive tool for surface analysis. Unfortunately, the quantitative interpretation of XPEEM images and spectra is not always straightforward, due to surface features and especially to experimental conditions which may vary from spectrum to spectrum and even within the same spectrum. In particular, the local density of impinging photons may change significantly over relevant acquisition times, thus modulating the photoelectron intensity.

In a recent article [9], we have described a novel approach for the analysis of XPEEM data, to map the nanoscale surface stoichiometry of binary alloys quantitatively. Here we develop a formal framework to extend the range of our analysis to almost arbitrarily complex alloys under non-ideal experimental conditions.

⁵ Authors to whom any correspondence should be addressed.

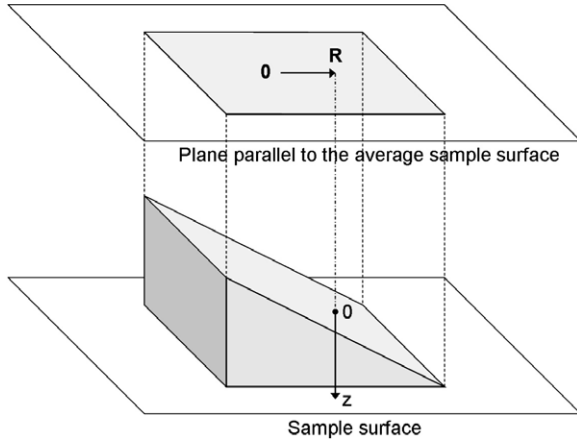


Figure 1. Representation of the system of spatial coordinates. Every point is described by two coordinates in a plane parallel to the average sample surface (which is parallel to the microscope focal plane), and one coordinate perpendicular to it, whose origin is chosen at the local sample surface.

2. Derivation of the analytical method

For the analysis of the photoemission data we define a convenient set of coordinates $\vec{r} \equiv (\vec{R}, z)$. As represented in figure 1, \vec{R} is a two-dimensional vector in a plane parallel to the average sample surface and z a coordinate along the direction perpendicular to the average sample surface. For notational convenience we set, for every \vec{R} , the origin of z at the surface of the specimen. z points downwards towards the bulk of the sample. A volume element dV reads $dV \equiv dS \times dz$ accordingly.

We consider the photoelectron intensity from the core level αA of the element A , emitted from a volume element $dV \equiv dS \times dz$ located at \vec{r} , in the infinitesimal energy range $(E - dE/2, E + dE/2)$:

$$dI_{\alpha A}(\vec{r}, E) = \wp(\vec{R}, E) \times \delta(\vec{R}) \Sigma_{\alpha A}(E) \rho C_A(\vec{r}) e^{-z/\lambda(E)} dV dE. \quad (1)$$

Here $\delta(\vec{R})$ is a geometric factor which accounts for the local orientation of the sample surface (i.e. relative x-ray illumination and aerial projection onto the focal plane); by $\Sigma_{\alpha A}(E) dE$ we denote the differential photoionization cross section for the photoelectrons emitted at kinetic energy E from the core level αA , at the photon energy chosen; ρ is the atomic density of the alloy (number of atoms per unit volume); $C_A(\vec{r})$ is the atomic fraction of element A within the alloy; and $\lambda(E)$ is the photoelectron escape depth at kinetic energy E . In principle $\lambda(E)$ can be adjusted by tuning the energy of the incident photons, so as to keep the kinetic energy of the photoemitted electrons constant, even among different core levels. Therefore, without loss of generality we assume that $\lambda(E) \equiv \lambda$ is a constant value. In most practical cases, however, adjusting the photon energy is unnecessary even among different core levels, due to the very broad minimum in the empirical plot of λ versus E [10].

The proportionality factor $\wp(\vec{R}, E)$ which links $dI_{\alpha A}(\vec{r}, E)$ to $\delta(\vec{R}) \Sigma_{\alpha A}(E) \rho C_A(\vec{r}) e^{-z/\lambda} dV dE$ accounts for the local photon density (x-ray intensity) impinging on point

\vec{R} while scanning through energy E under the particular conditions realized in the experiment, and for other terms that depend on the specific experimental set-up (e.g. transmission of the microscope, characteristics of the detector, etc). $\wp(\vec{R}, E)$ modulates non-homogeneously the characteristic shape of the spectrum as defined by $\Sigma_{\alpha A}(E)$, in a way which may vary from experiment to experiment (e.g. due to drift or even loss of the impinging photon beam).

After background subtraction (see [11]), we first integrate over the various measured photoelectron energies of core level αA , to extract the total elastic contribution from αA from dV . We assume that the integral is extended over a finite kinetic energy interval $\Delta E_{\alpha A}$ (typically a few eV broad). Then

$$dI_{\alpha A}(\vec{r}) = \mathfrak{S}_{\alpha A}(\vec{R}, \Delta E_{\alpha A}) \times \delta(\vec{R}) \rho C_A(\vec{r}) e^{-z/\lambda} dV, \quad (2)$$

with

$$\mathfrak{S}_{\alpha A}(\vec{R}, \Delta E_{\alpha A}) = \int_{\Delta E_{\alpha A}} dE \wp(\vec{R}, E) \times \Sigma_{\alpha A}(E). \quad (3)$$

Equation (3) embeds the information from both the intrinsic photoemission physics via $\Sigma_{\alpha A}(E)$ and from the extrinsic experimental conditions via $\wp(\vec{R}, E)$. Significantly, it is independent of both the chemical composition $C_A(\vec{r})$ and the depth z .

The specific analytical structure of $\mathfrak{S}_{\alpha A}(\vec{R}, \Delta E_{\alpha A})$ represents a critical issue. Under ideal conditions of uniform illumination (over space and time), one may recover $\mathfrak{S}_{\alpha A}(\vec{R}, \Delta E_{\alpha A}) = \wp \times \int_{\Delta E_{\alpha A}} dE \Sigma_{\alpha A}(E) = \wp \times \sigma_{\alpha A}$, which may enable the use of tabulated values for the cross section $\sigma_{\alpha A}$ in a quantitative comparison among different core levels. However, especially in spectromicroscopy experiments, ideal conditions are not easily met. Therefore we propose an algorithm to overcome this problem.

Integrating equation (2) over the z coordinate gives

$$dI_{\alpha A}(\vec{R}) = \mathfrak{S}_{\alpha A}(\vec{R}, \Delta E_{\alpha A}) \times \delta(\vec{R}) \rho \lambda c_A(\vec{R}) dS, \quad (4)$$

where we have defined the concentration of element A averaged over the direction perpendicular to the surface with the exponential weight $e^{-z/\lambda}$:

$$c_A(\vec{R}) \equiv \frac{\int_0^{\infty} dz C_A(\vec{r}) e^{-z/\lambda}}{\lambda}. \quad (5)$$

Equation (5) shows that λ defines the depth scale of the probed region.

Now we assume that the sample surface has features of the type displayed in figure 2, with a number of inhomogeneous patches embedded in a homogeneous matrix, whose geometric orientation and chemical composition are constant (the latter may be yet unknown *ab initio*). This matrix spans over the set of surface points S^m , e.g. the *basal* plane in figure 2. The whole sample consists of an N -ary alloy, whose components have concentrations $c_n(\vec{R})$, $1 \leq n \leq N$, averaged in z using equation (5).

The *homogeneous* matrix is characterized by the chemical composition

$$c_n(\vec{R}) = c_n^m \quad 1 \leq n \leq N, \quad \sum_{i=1}^N c_i^m = 1; \quad (6)$$

$$\forall \vec{R} \in S^m,$$

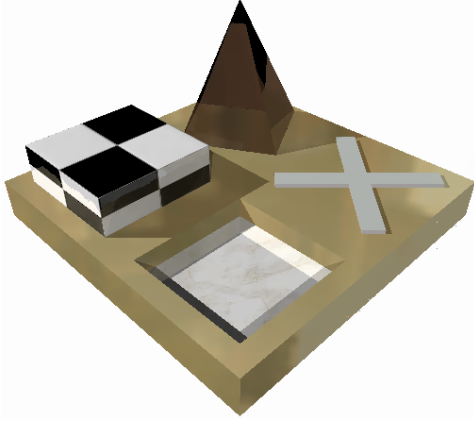


Figure 2. Schematic representation of the several types of surface targeted by our approach. In this example we consider: a cross, for example marked lithographically; a pit, for example etched chemically; a mesa; and a pyramid, possibly inhomogeneous and for example grown epitaxially, embedded in a chemically and morphologically homogeneous matrix.

and by the geometrical factor

$$\delta(\vec{R}) = \delta^m; \quad \forall \vec{R} \in S^m. \quad (7)$$

Within the *inhomogeneous* patches the chemical composition is only required to comply with the general condition $\sum_{i=1}^N c_i(\vec{R}) = 1$. Both $c_n(\vec{R})$ and $\delta(\vec{R})$ exhibit an arbitrary dependence on \vec{R} anywhere outside the homogeneous matrix.

We now suppose that the overall photoelectron intensities (integrated elastic signals) have been retrieved for one core level $\alpha|_n n$ ($1 \leq n \leq N$) from each of the N elements, and this throughout the surface. Such an operation implies the ability to associate the measured photoelectron flux to specific αA core levels, which may require the use of fitting routines.

From the experimental data we construct homogeneous matrix elastic intensity maps. To this end we first delete all inhomogeneous areas from the original images. In a second step, these empty areas are filled with values obtained from the homogeneous matrix by interpolation. In this way, we are left with two sets of images: the measured elastic maps from the actual sample, $dI_{\alpha|_n n}(\vec{R}) (= \mathfrak{S}_{\alpha|_n n}(\vec{R}, \Delta E_{\alpha|_n n}) \times \delta(\vec{R}) \rho \lambda c_n(\vec{R}) dS)$; plus the calculated elastic maps obtained by interpolation, under the same experimental conditions, $dI_{\alpha|_n n}^m(\vec{R}) (= \mathfrak{S}_{\alpha|_n n}(\vec{R}, \Delta E_{\alpha|_n n}) \times \delta^m \rho \lambda c_n^m dS)$. Here, it is crucial that the numerical procedure leads to the identity of the factors $\mathfrak{S}_{\alpha|_n n}(\vec{R}, \Delta E_{\alpha|_n n})$ in the two expressions. So, in order to decouple the analysis from the experimental factors represented in $\wp(\vec{R}, E)$, and thus in $\mathfrak{S}_{\alpha|_n n}(\vec{R}, \Delta E_{\alpha|_n n})$, we take the ratios of these two sets of images:

$$r_{\alpha|_n n}(\vec{R}) \equiv \frac{dI_{\alpha|_n n}(\vec{R})}{dI_{\alpha|_n n}^m(\vec{R})} = \begin{cases} \frac{\delta(\vec{R}) c_n(\vec{R})}{\delta^m c_n^m} & 1 \leq n < N \\ \frac{\delta(\vec{R}) \left(1 - \sum_{i=1}^{N-1} c_i(\vec{R})\right)}{\delta^m \left(1 - \sum_{i=1}^{N-1} c_i^m\right)} & \{n = N\}. \end{cases} \quad (8)$$

Substituting the first $N - 1$ equations into the last one leads to a parametric function of these ratios:

$$r_{\alpha|_N N}(\vec{R}) = \frac{\frac{\delta(\vec{R})}{\delta^m} - \vec{c}^m \cdot \vec{r}_\alpha(\vec{R})}{1 - \text{sum}(\vec{c}^m)} \equiv H_{\vec{c}^m} \left(\frac{\delta(\vec{R})}{\delta^m}, \vec{r}_\alpha(\vec{R}) \right). \quad (9)$$

Here we have defined the $(N - 1)$ -dimensional vectors \vec{c}^m and $\vec{r}_\alpha(\vec{R})$, whose n th components are c_n^m and $r_{\alpha|_n n}(\vec{R})$, respectively. The two operators \cdot and sum denote the scalar product between two vectors and the sum of the elements of a vector, respectively. When the ratios of the geometric factors are known, equation (9) can be used to extract the matrix chemical composition \vec{c}^m (e.g. in an algebraic system with N equations). However, here we propose a more general solution, which requires yet one more assumption. We assume that the geometric factors are constant in a set of points $S^{\tilde{\delta}}$ outside the homogeneous matrix, where $\delta(\vec{R}) \equiv \tilde{\delta}$. For instance, in figure 2 $S^{\tilde{\delta}}$ may contain the cross, the pit, and the mesa, but not the pyramid (in this example $\tilde{\delta} = \delta^m$). $S^{\tilde{\delta}}$ may be associated for example to a repeated pattern (either self-assembled or artificial). Within $S^{\tilde{\delta}}$, equation (9) becomes $H_{\vec{c}^m}(\frac{\tilde{\delta}(\vec{R})}{\delta^m}, \vec{r}_\alpha(\vec{R})) \equiv h_{\frac{\tilde{\delta}}{\delta^m}, \vec{c}^m}(\vec{r}_\alpha(\vec{R}))$, which is a hyperplane in the N -dimensional space $(r_{\alpha|_N N}(\vec{R}), \vec{r}_\alpha(\vec{R}))$, parametric in the set of N variables $(\frac{\tilde{\delta}}{\delta^m}, \vec{c}^m)$. By measuring $r_{\alpha|_N N}(\vec{R})$ and $\vec{r}_\alpha(\vec{R})$ for a sufficiently large number ($> N$) of points in $S^{\tilde{\delta}}$, one can use equation (9) in a least-squares fit where $(\frac{\tilde{\delta}}{\delta^m}, \vec{c}^m)$ is taken as the vector of free parameters. This gives as a result the matrix chemical composition \vec{c}^m . For each inhomogeneous patch one can finally obtain

$$c_n(\vec{R}) = \frac{\delta^m}{\delta(\vec{R})} r_{\alpha|_n n}(\vec{R}) c_n^m \quad 1 \leq n \leq N. \quad (10)$$

Equation (10) can be used to obtain the laterally resolved elemental composition within the cross, the pit, and the mesa, as well as the pyramid, in figure 2.

Further immediate manipulation of equation (10) leads to a significant simplification of the problem:

$$c_n(\vec{R}) = \frac{c_n(\vec{R})}{\sum_{i=1}^N c_i(\vec{R})} = \frac{r_{\alpha|_n n}(\vec{R}) c_n^m}{\sum_{i=1}^N r_{\alpha|i i}(\vec{R}) c_i^m} \quad 1 \leq n \leq N. \quad (11)$$

Here we have dropped any reference to the geometric factors of the surface, which may be difficult to access experimentally, especially in areas partly shadowed from the x-rays. Thanks to equation (11), the only morphological information required is: (1) the existence of a chemically and geometrically homogeneous matrix S^m ; and (2) the existence of another geometrically homogeneous area $S^{\tilde{\delta}}$. However, we caution the reader that in some cases the set $S^{\tilde{\delta}}$ may be unidentifiable, and then the ability to calculate the geometric factors from the surface orientation is necessary.

One way to estimate the geometric factors was reported by Heun and co-workers [12]. Suppose that the surface is irradiated with an x-ray beam, whose direction is determined by the unit vector \hat{k} . By manipulation of the concepts

demonstrated in [12], the geometric factor for each fraction S of the sample surface assumes the very simple form

$$\delta(S) = -\hat{k} \cdot \int_S dS \hat{n}(dS)/S, \quad (12)$$

where $\hat{n}(dS)$ is the normal unit vector of the surface element dS , pointing outwards from the sample. In the limit $S \rightarrow dS$ we can write $\delta(dS) \equiv \delta(\vec{R})$, by identifying the surface element with the two-dimensional vector in the plane parallel to the average sample surface. In this way $\delta(\vec{R}) = -\hat{k} \cdot \hat{n}(\vec{R})$.

Alternative methods in use in the breakdown of spectra include the principal component analysis (PCA) [13–16]. In this context the PCA consists in computing the eigenvectors of a covariance matrix constructed from a set of measured spectra, which allows us to retrieve their projections onto so-called *principal components*. Generally the latter are linear combinations of *physical components*. To use the PCA to quantify the chemical composition of the sample, the principal components must be interpreted, for example by the use of reference spectra. Other strategies currently employed in the analysis of spectra start from equation (1) for a *direct* comparison of photoelectron intensities from different elements [17]. This generally requires the use of tabulated parameters, such as the cross sections for the photoemission processes investigated. Moreover, in XPEEM (and in photoelectron spectroscopy in general) a direct comparison of spectra from different chemical species entails ideal experimental conditions, which translates in our terms into $\mathfrak{S}_{\alpha A}(\vec{R}, \Delta E_{\alpha A}) = \wp \times \sigma_{\alpha A}$. When the photon beam is well uniform and stable, this is a reasonable approximation.

3. Application of the method: a model example

As an example of the potential of our analytical tool we illustrate the surface chemical mapping of a complex system. The focus of this paragraph is on the procedure adopted to retrieve the quantitative information on the elemental composition of the surface. We will show how the formalism described in the previous paragraph can be brought to fruition in a real situation. The samples analysed are: (a) a Au-patterned Si(100) surface; and (b) a nanostructured surface obtained by deposition of Ge on (a). This results in the lateral ordering of three-dimensional quantum dots, which holds the promise of great technological impact [18, 19]. However, here we emphasize the chemical mapping only. Details on sample preparation and data acquisition are given in [19]. Samples were characterized *in situ* using XPEEM at a photon energy of 195 eV. The best lateral resolution of the microscope is ~ 30 nm [9]. Here we acquired micrographs at a lower lateral resolution, to improve the photoelectron signal-to-noise ratio. The depth sensitivity is 0.5 nm in our experimental conditions.

3.1. Two-element system (Au/Si)

Sample (a) was prepared by deposition of ~ 1 nm of Au on a hydrogen-passivated Si(001) surface through a silicon nitride stencil mask with arrays of 200×200 nm² square

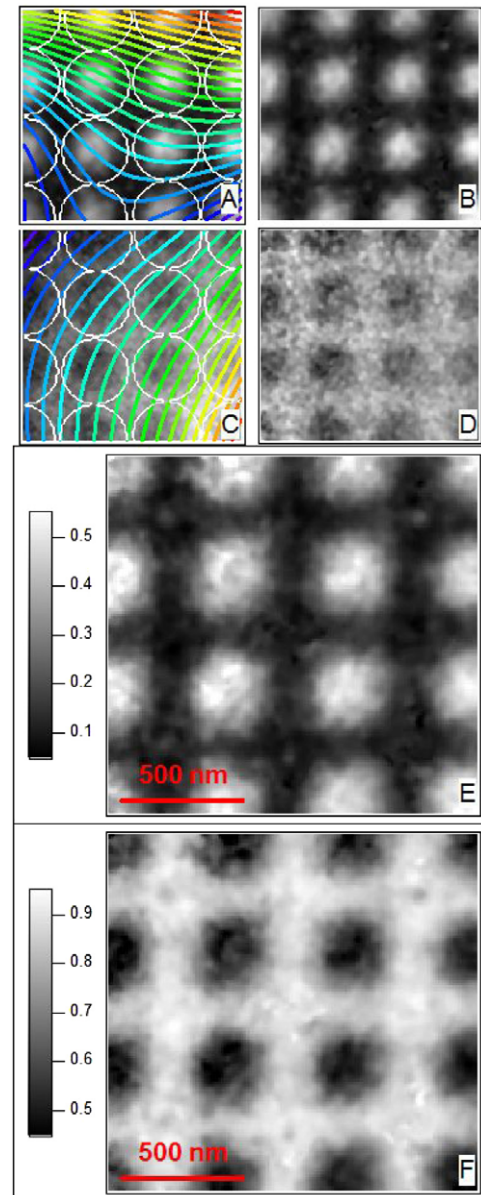


Figure 3. Analysis of elastic intensity maps from Au 4f and Si 2p core levels. Original maps with contour plots of the simulated *homogeneous matrix* maps (Au A, Si C); so-called intensity ratios (Au B, Si D); chemical maps (Au E, Si F).

windows [19]. We describe the analysis of the XPEEM data by the system of equations presented in the previous paragraph. We assume the surface to be composed of two distinct areas with equivalent orientation: a homogeneous matrix in the region between the Au pads (indeed far enough from the Au pads); and some chemically inhomogeneous patches in the regions at and close to the Au pads. The former is treated as the basal plane in figure 2; the latter is represented by either the cross, the pit or the mesa in figure 2. The analytical process is represented in figure 3. From the recorded Au 4f and Si 2p images and spectra we calculated elastic intensity maps (3(A) and (C) for Au and Si, respectively). The intensity in the region far enough from the Au pads (outside of the white circles) is

interpolated throughout the entire field of view⁶. The process is represented in the contour plots in figures 3(A) and (C). A strong lateral variation in intensity is quite evident in these maps, most likely caused by an inhomogeneous illumination. By taking the ratios between the original intensity maps and the simulated homogeneous matrix intensity maps, we constructed $r_{\text{Au } 4f}(\bar{R})$ and $r_{\text{Si } 2p}(\bar{R})$ images (figures 3(B) and (D) for Au and Si). With the assumptions above and the notation in the previous paragraph, S^{δ} can be taken as the entire surface, and $\delta = \delta^m$. Equation (9) then simply translates into

$$r_{\text{Au } 4f}(\bar{R}) = \frac{1 - r_{\text{Si } 2p}(\bar{R})c_{\text{Si}}^m}{1 - c_{\text{Si}}^m}. \quad (13)$$

The calculated $r_{\text{Au } 4f}(\bar{R})$ and $r_{\text{Si } 2p}(\bar{R})$ from throughout the surface were used in a (*linear*) fit to extract the Si content in the homogeneous matrix c_{Si}^m .

Equation (11) finally gives the stoichiometry everywhere at the surface:

$$c_{\text{Si}}(\bar{R}) = \frac{r_{\text{Si } 2p}(\bar{R})c_{\text{Si}}^m}{r_{\text{Si } 2p}(\bar{R})c_{\text{Si}}^m + r_{\text{Au } 4f}(\bar{R})(1 - c_{\text{Si}}^m)}; \quad (14)$$

$$c_{\text{Au}}(\bar{R}) = 1 - c_{\text{Si}}(\bar{R}).$$

We note that, in this two-element system, within the Au pads equations (13) and (14) read $c_{\text{Si}}(\bar{R}) = \frac{r_{\text{Au } 4f}(\bar{R}) - 1}{(r_{\text{Au } 4f}(\bar{R})/r_{\text{Si } 2p}(\bar{R})) - 1}$, which is the solution given in [20]. In this latter form no fitting procedure is required to infer the homogeneous matrix composition (in [20] the wetting layer composition). We suggest that whenever possible this simplified formulation may be preferred, which is expected to give more accurate values, the propagation of fitting uncertainties being avoided⁷.

Equation (14) was used to obtain chemical maps of the Au-patterned sample, as shown in figures 3(E) and (F). We caution the reader that due to the physics of the photoemission process we cannot distinguish between a homogeneously mixed alloy ($\text{Au}_x\text{Si}_{1-x}$) and a layered structure (Au on Si). Our result is therefore a weighted average of the individual compositions of the topmost layers, according to equation (5).

The Au pads are clearly visible in the chemical maps (bright and dark spots in the Au and Si maps in figures 3(E) and (F), respectively). A small, but non-negligible fraction of Au is also found in between the pads. We emphasize that the occurrence of this fraction is essential to apply our analytical approach (see equation (13)).

3.2. Three-element system (Ge/Au/Si)

Further complexity was added by deposition of ~ 7 ML (0.07 ML min^{-1}) of Ge at 450°C onto the Au-patterned Si(100) surface. The deposition of Ge resulted in the nucleation and growth of three-dimensional nanostructures, located between the original Au pads [19].

⁶ This was achieved *computationally* from the original elastic intensity maps in two steps: first we deleted the Au pad regions, and then we filled these empty areas with values obtained by interpolation from regions far away from the Au pads.

⁷ On the other hand the simplified equations do not allow us to access the stoichiometry of the homogeneous matrix directly.

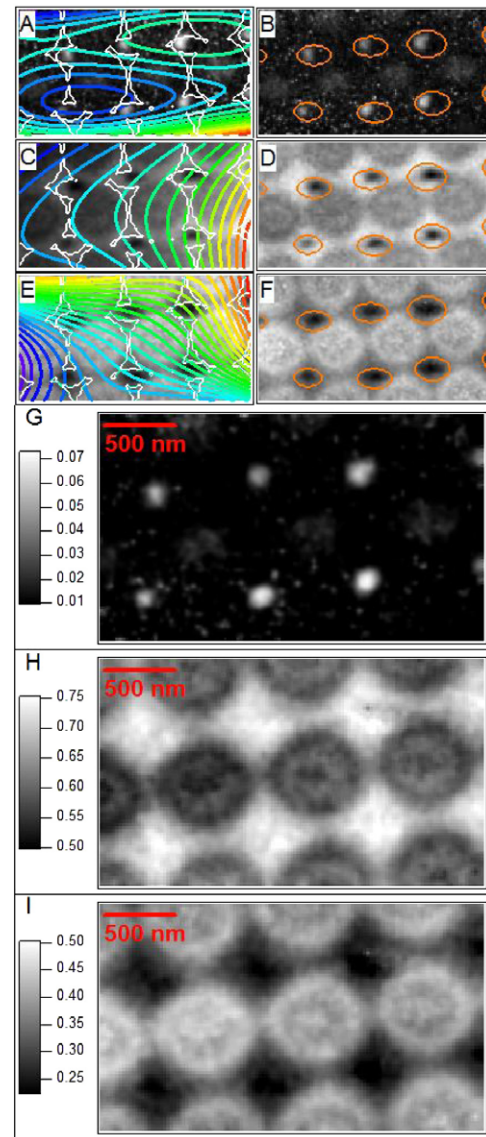


Figure 4. Analysis of elastic intensity maps from Au 4f, Ge 3d and Si 2p core levels. Original maps with contour plots of the simulated *homogeneous matrix* maps (Au A, Ge C, Si E); so-called intensity ratios (Au B, Ge D, Si F); chemical maps (Au G, Ge H, Si I).

At this stage, the morphology of the sample can be sketched as follows: first, there is a chemically and morphologically homogeneous matrix in the regions far enough from both the Au pads and the three-dimensional islands, which is like the basal plane in figure 2. Next, there are chemically inhomogeneous areas corresponding to the Au pads, with a morphology equivalent to the homogeneous matrix, which are treated as the cross, the pit or the mesa in figure 2. Finally, there are also chemically and morphologically inhomogeneous areas, associated to the three-dimensional nanostructures, which are schematically represented by the pyramid in figure 2. Figure 4 shows our analytical process. Au 4f, Ge 3d and Si 2p images and spectra were used to compute the elastic intensity maps given in panels 4(A), (C) and (E) for Au, Ge and Si, respectively. From these images we simulated the homogeneous matrix elastic

intensity maps throughout the field of view (by first erasing the Au pads, the islands and their shadows, which leaves the areas enclosed in the white perimeters only). The interpolated homogeneous matrix maps are represented in the contour plots superimposed in 4(A), (C) and (E). These are used to define $r_{\text{Au } 4\text{f}}(\bar{R})$, $r_{\text{Ge } 3\text{d}}(\bar{R})$ and $r_{\text{Si } 2\text{p}}(\bar{R})$, shown in 4(B), (D) and (F). Afterwards we selected areas of the sample with an equivalent and suitable morphology. For convenience we identify S^{δ} as the whole of the regions between the Au pads far enough from the three-dimensional islands and their shadows, and of the regions related to the Au pads (i.e. as the entire surface with the exclusion of the emerging nanostructures and their shadows). S^{δ} is shown as the area outside of the orange ovals in figures 3(B), (D) and (F). With such a choice $\tilde{\delta} = \delta^m$. Within S^{δ} the intensity ratios must satisfy equation (9), which reads

$$r_{\text{Ge } 3\text{d}}(\bar{R}) = \frac{1 - r_{\text{Au } 4\text{f}}(\bar{R})c_{\text{Au}}^m - r_{\text{Si } 2\text{p}}(\bar{R})c_{\text{Si}}^m}{1 - c_{\text{Au}}^m - c_{\text{Si}}^m}, \quad (15)$$

which is a plane in the $(r_{\text{Ge } 3\text{d}}, r_{\text{Au } 4\text{f}}, r_{\text{Si } 2\text{p}})$ space. This can be used in a fit to determine the homogeneous matrix stoichiometry, defined by c_{Au}^m and c_{Si}^m . With these c_{Au}^m and c_{Si}^m from equation (15), we can finally use equation (11) to calculate the chemical composition everywhere:

$$\begin{aligned} c_{\text{Au}}(\bar{R}) &= \frac{r_{\text{Au } 4\text{f}}(\bar{R})c_{\text{Au}}^m}{r_{\text{Au } 4\text{f}}(\bar{R})c_{\text{Au}}^m + r_{\text{Si } 2\text{p}}(\bar{R})c_{\text{Si}}^m + r_{\text{Ge } 3\text{d}}(\bar{R})(1 - c_{\text{Au}}^m - c_{\text{Si}}^m)}; \\ c_{\text{Si}}(\bar{R}) &= \frac{r_{\text{Si } 2\text{p}}(\bar{R})c_{\text{Si}}^m}{r_{\text{Au } 4\text{f}}(\bar{R})c_{\text{Au}}^m + r_{\text{Si } 2\text{p}}(\bar{R})c_{\text{Si}}^m + r_{\text{Ge } 3\text{d}}(\bar{R})(1 - c_{\text{Au}}^m - c_{\text{Si}}^m)}; \\ c_{\text{Ge}}(\bar{R}) &= 1 - c_{\text{Au}}(\bar{R}) - c_{\text{Si}}(\bar{R}). \end{aligned} \quad (16)$$

The set of equations (16) was used to obtain images such as those in figures 4(G)–(I) for Au, Ge, and Si, respectively.

Our results reveal that the pattern of the chemical composition of the surface is rather complex. Here we do not aim at a discussion of the rich phenomenology related to the diffusion dynamics in this system. Rather, we wish to draw attention to the importance of our chemical maps. In particular, we emphasize that there is no alternative tool able to give results on the nanoscale surface composition with an overall quality comparable to our maps. The kind of analysis developed herein allows us to access a wealth of phenomenological information which may be otherwise unattainable.

Here we have demonstrated that our novel analytical process can be successfully and conveniently brought to fruition. We have illustrated the steps necessary to produce reliable chemical maps of surfaces by XPEEM, through an example of considerable complexity. The model application in this paper may serve as a guide to exploit our approach in the study of a wealth of surfaces with chemical inhomogeneities, particularly at the nanoscale. We anticipate that a variety of inspiring and functional phenomena may be elucidated by use of our analytical paradigm.

Acknowledgments

F Ratto acknowledges the ICCS-CBIE, FQRNT and FQRNT-MELS (Quebec) for graduate fellowships that supported this work. F Rosei acknowledges funding from NSERC of Canada, and salary support from FQRNT and the Canada Research Chairs program. O Moutanabbir acknowledges JSPS (Japan) and K M Itoh for their support. We are very grateful to J T Robinson, A Locatelli, T O Mentès and L Aballe for their help with the acquisition of the experimental data, which prompted the development of this approach.

References

- [1] Rosei F 2004 Nanostructured surfaces: challenges and frontiers in nanotechnology *J. Phys.: Condens. Matter* **16** 1373
- [2] Ratto F, Costantini G, Rastelli A, Schmidt O G, Kern K and Rosei F 2006 Alloying of self-organized semiconductor 3D islands *J. Exp. Nanosci.* **1** 279
- [3] Motta N 2002 Self assembling and ordering of Ge/Si(111) quantum dots: scanning microscopy probe studies *J. Phys.: Condens. Matter* **14** 8353
- [4] Teichert C 2002 Self-organization of nanostructures in semiconductor heteroepitaxy *Phys. Rep.* **365** 335
- [5] Grill L 2008 Functionalized molecules studied by STM: motion, switching and reactivity *J. Phys.: Condens. Matter* **20** 053001
- [6] Gruverman A and Kholkin A 2006 Nanoscale ferroelectrics: processing, characterization and future trends *Rep. Prog. Phys.* **69** 2443
- [7] Aiken J D and Finke R G 1999 A review of modern transition-metal nanoclusters: their synthesis, characterization, and applications in catalysis *J. Mol. Catal. A* **145** 1
- [8] Huang X J and Choi Y K 2007 Chemical sensors based on nanostructured materials *Sensors Actuators B* **122** 659
- [9] Ratto F, Locatelli A, Fontana S, Kharrazi S, Ashtaputre S, Kulkarni S K, Heun S and Rosei F 2006 Chemical mapping of individual semiconductor nanostructures *Small* **2** 401
- [10] Tanuma S, Powell C J and Penn D R 1991 Calculations of electron inelastic mean free paths. II. Data for 27 elements over the 50–2000 eV range *Surf. Interface Anal.* **17** 911
- [11] Ratto F, Rosei F, Locatelli A, Cherifi S, Fontana S, Heun S, Szkutnik P D, Sgarlata A, De Crescenzi M and Motta N 2005 Composition of single Ge(Si) islands in the growth of Ge on Si(111) by x-ray spectromicroscopy *J. Appl. Phys.* **97** 043516
- [12] Heun S, Watanabe Y, Ressel B, Bottomley D, Schmidt T and Prince K C 2001 Core-level photoelectron spectroscopy from individual heteroepitaxial nanocrystals on GaAs(001) *Phys. Rev. B* **63** 125335
- [13] Sastry M 1997 Application of principal component analysis to x-ray photoelectron spectroscopy—the role of noise in the spectra *J. Electron Spectrosc. Relat. Phenom.* **83** 143
- [14] Francis P J and Wills B J 1999 *Introduction to Principal Components Analysis (ASP Conf. Series 162: Quasars and Cosmology)* ed G J Ferland and J A Baldwin (San Francisco, CA: Astronomical Society of the Pacific) p 363
- [15] Gaarenstroom S W 1979 Chemical characterization from carbon Auger spectra by application of pattern recognition and factor analysis *J. Vac. Sci. Technol.* **16** 600
- [16] Gaarenstroom S W 1981 Principal component analysis of Auger line shapes at solid–solid interfaces *Appl. Surf. Sci.* **7** 7
- [17] Biasiol G, Heun S, Golinelli G B, Locatelli A, Mentès T O, Guo F Z, Hofer C, Teichert C and Sorba L 2005 Surface compositional gradients of InAs/GaAs quantum dots *Appl. Phys. Lett.* **87** 223106

- [18] Robinson J T, Liddle J A, Minor A, Radmilovic V, Yi D O, Greaney P A, Long K N, Chrzan D C and Dubon O D 2005 Directed assembly of semiconductor island arrays by surface diffusion patterning *Nano Lett.* **5** 2070
- [19] Robinson J T, Ratto F, Moutanabbir O, Heun S, Locatelli A, Montes T O, Aballe L and Dubon O D 2007 Gold-catalyzed oxide nanopatterns for the directed assembly of Ge island arrays on Si *Nano Lett.* **7** 2655
- [20] Ratto F, Rosei F, Locatelli A, Cherifi S, Fontana S, Heun S, Szkutnik P D, Sgarlata A, De Crescenzi M and Motta N 2004 Composition of single Ge(Si) islands in the growth of Ge on Si(111) *Appl. Phys. Lett.* **84** 4526